Contact and stress anisotropies in start-up flow of colloidal suspensions

Nicos S. Martys,[1] Didier Lootens,[2] William George,[1] and Pascal Hébraud[3]
[1]*National Institute of Standards and Technology, 100 Bureau Drive, Stop 8615, Gaithersburg, Maryland 20899-8615, USA*
[2]*SIKA Technology A.G., Tuffenwies 16, CH-8048 Zürich, Switzerland*
[3]*IPCMS, UMR 7504, 23 rue du Loess, 67034 Strasbourg Cedex 02, France*
(Received 25 August 2008; revised manuscript received 22 April 2009; published 11 September 2009)

Spatiotemporal correlations in start-up flows of attractive colloids are explored by numerical simulations as a function of their volume fraction and shear rate. The suspension is first allowed to flocculate during a time t_w, then the stress necessary to induce its flow is computed. We find that, at low volume fractions, the stress is a universal function of the strain. On the contrary, at high volume fractions, this scaling behavior is no longer observed and a supplementary stress becomes necessary to induce flow. To better understand the physical origin of the supplementary stress, we examine the creation, disruption, and orientation of contacts between the particles and the corresponding contribution to stress as a function of strain. Our simulations show that the onset of flow is dominated by the creation of contacts between the particles at low shear rates and by their disruption at high shear rates. However, neither the evolution of the number of contacts with strain nor their orientation can fully account for the nonscaling behavior of the stress at high volume fractions. At small strains, the relative importance of forcing in the compression quadrant increases with volume fraction and with flocculation time. This mechanism of stress transmission through the compression quadrant is not accounted for in the usual description of yield stress, which considers the breaking of bonds oriented in the extension quadrant.

DOI: 10.1103/PhysRevE.80.031401 PACS number(s): 83.80.Hj, 83.60.Df, 87.10.Tf

I. INTRODUCTION

Many complex fluids such as dense suspensions, emulsions, or colloidal glasses are composed of interacting particles that self-organize into an isotropic microstructure under quiescent conditions. The application of a rate of deformation disrupts this isotropy such that a collective behavior emerges. As a consequence, a rich variety of structures emerges [1–3], which determines mechanical macroscopic flow properties characterized by nonlinear relationships between the stress and the shear rate: among them, plastic behavior [4] (a power-law relationship between the stress and the shear rate), jamming [5–7] (flow stops under the application of a high enough stress), and yielding [8] (flow does not start although a nonzero small stress is applied). It is of crucial importance to understand how these materials start to flow and to tune their physicochemical properties in order to reduce the amount of energy necessary to make them flow. An outstanding question about such systems thus emerges: what physical mechanisms are responsible for the observed macroscopic behavior as the initial isotropy is broken? For example, mechanical measurements reveal a very nonlinear relationship between the applied stress and the induced shear strain or shear rate: it is necessary to apply a nonzero value of the stress, the yield stress, in order to induce the flow. The microscopic origin of the yield stress is not generally understood, and its value, its measurement, and even its existence are not well established [9,10]. The yield stress is generally thought as a manifestation of the maximum force needed to break contacts between particles [4]. But, when a suspension flows, particles are not only drawn apart but also pushed together. That is, under simple shear, two colloids whose center-to-center segment is oriented in the extension quadrant are drawn apart, whereas when they approach each other due to the flow, their center-to-center segment is oriented in the compression quadrant (Fig. 1). In this paper, we show that this phenomenon leads to a physical mechanism that produces an excess of stress at small strains. Indeed, as flow develops, aggregates of particles form [11–13]. These aggregates are not isotropic, and their orientation relative to the flow direction depends on the shear rate and the volume fraction of the suspension, as may be seen from direct observation of the particles inside the shear cell (Fig. 2). We show that, at high volume fraction, a supplementary stress develops at the onset of flow. This supplementary stress is due to the organization of contacts between particles in the compression quadrant of the shear flow, and it is not fully accounted for by the simple breaking of colloidal contacts.

The paper is organized as follows. The computational model is briefly introduced and the preparation of the sus-

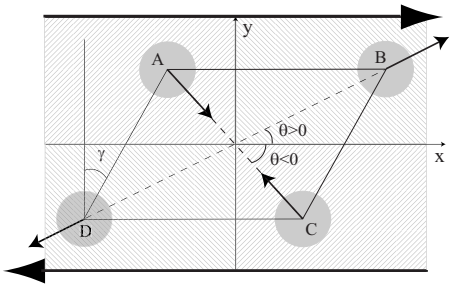

FIG. 1. Strain of a square under a simple shear. Particles *A* and *C*, whose center-to-center segment lies in the compression quadrant (hatching along the first diagonal), are drawn together due to the flow, whereas particles *B* and *D*, in the extension quadrant (hatching along the second diagonal), are pulled apart. θ is the angle of the center-to-center segment and the direction of the flow.

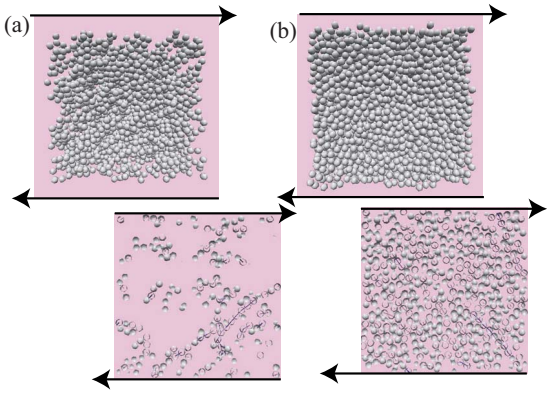

FIG. 2. (Color online) Images from a simulation of a sheared colloidal suspension for volume fractions (a) ϕ=0.20 and (b) ϕ =0.50 and at a strain γ of about 0.5. All views are in the shear gradient plane with the top of the suspension moving to the right and the bottom moving to the left. The figures, offset to the lower right, represent a typical slice through the respective suspension. Included in the lower images is an indication of stress chains where the largest stresses are found. Note that for the ϕ=0.20, the chains form in the extension quadrant. In contrast, for the ϕ=0.50 case, many chains are formed both in extension and compression. Typically, at the lowest shear rates there are fewer stress chains in compression, however there are more by proportion as the volume fraction and shear rate are increased.

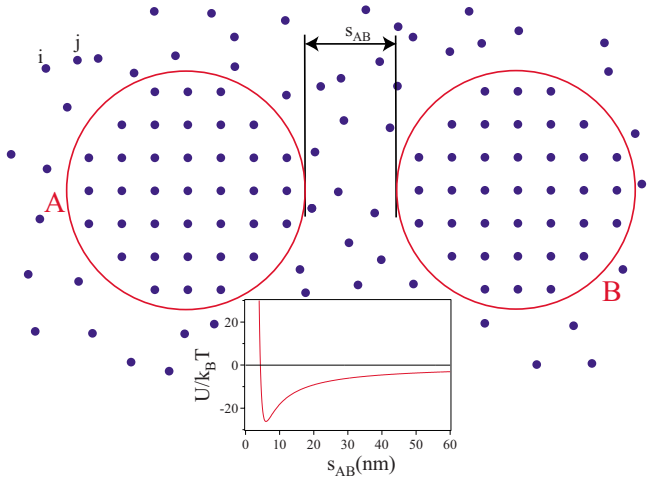

FIG. 3. (Color online) Definition of the DPD particles and of the colloids. The suspension fluid is represented by DPD particles (full disks). *A* and *B* are two colloids that consist of an assembly of DPD particles, subjected to constraints so that they form a rigid body. In addition to the DPD based forces between all (DPD) particles, colloids *A* and *B* are subjected to van der Waals repulsive force and lubrication forces. *Inset*: additional interaction potential between the colloids (Derjaguin approximation of a Lennard-Jones potential).

pension, before the application of shear, is described. A constant shear is then applied and it is shown that, at low concentrations, the growth of stress with strain exhibits a universal behavior. This universal behavior is not observed at small strains and the higher concentration studied. Indeed, an additional stress, supplementary to that indicated by simple scaling arguments, is needed to make the suspension flow. The microstructure of the suspension responsible of this supplementary stress is then investigated in the last part of the paper, where the orientations of pairs of particles in contact and the stresses between them are studied.

II. DISSIPATIVE PARTICLE DYNAMICS MODEL

We use a dissipative particle dynamics (DPD) based model [14] to study the onset of flow of a colloidal suspension of attractive particles. This approach can be thought of as a Lagrangian formulation of Navier Stokes with thermal fluctuations [15]. As this computational model is largely described in a previous work [14], we will only highlight its main features and focus, more so, on the relevant aspects of the model to this work. The DPD simulation is similar in structure to molecular dynamics simulation, but, instead of modeling all the molecular properties of the system, the motion of mesoscopic DPD particles that represent a coarse grained fluid is considered [14,16] (Fig. 3). The DPD particles are subjected to conservative, dissipative, and random forces [17],

$$\mathbf{F}_{ij} = \mathbf{F}_{ij}^{C} + \mathbf{F}_{ij}^{D} + \mathbf{F}_{ij}^{R}. \tag{1}$$

The conservative force is a soft repulsive radial force, which decreases linearly with the center-to-center distance, $|\mathbf{r}_i - \mathbf{r}_j|$, between the two DPD particles i and j and whose amplitude is chosen so that the compressibility of the DPD fluid matches that of water. The dissipative force is proportional to the difference of velocities between DPD particles i and j, $\mathbf{v}_i - \mathbf{v}_j$, and acts to slow down their relative motion, producing a viscous effect. Lastly, a random force is added, which controls the temperature of the system. The dissipative and random forces control the viscosity of the fluid and, to maintain a well-defined temperature, are related by fluctuation-dissipation theorem [18]. In contrast to the individual DPD particles, a colloid is then defined as an assembly of constrained DPD particles so that they form a rigid body (Fig. 3). As described previously [14,19], when modeling a dense suspension of hard spheres (or colloids in our case), the DPD particle interactions are not sufficiently strong to prevent overlaps of the spheres so this model includes lubrication forces [14,20]. The computational model, employed in this study, has been shown to recover the Einstein intrinsic viscosity for a dilute suspension of spheres [14,16], reasonable estimates of the Huggins coefficient for moderately dense suspension [14,19], and good agreement with Stokesian dynamics predictions of relative viscosity as a function of shear rate in dense suspensions [14,21].

For this study, an additional interaction potential is incorporated into the model. Here, we use a Derjaguin-type approximation of the Lennard-Jones interactions [22] between colloid spheres A and B at short distances. This potential scales as the sum of a hard-sphere repulsion term, $A_{\mathrm{HS}}/s_{AB}^{7}$, and a van der Waals potential, H/s_{AB}, where A_{HS} and H are constants related to the hard-sphere potential and to the Hamaker constant and s_{AB} is the distance between the two particles surfaces. The colloid's radius is the only length scale explicitly included in the description of the suspension. The parameters chosen for the simulation could correspond to

spherical alumina particles of approximately 100 nm diameter. The interaction potential between two particles exhibits a minimum of $25k_BT$ at a distance of 6 nm between the surfaces of the particles. The time integration scheme for the DPD particles and the colloids is based on a velocity-Verlet algorithm described in [14,23].

The stress tensor for this model suspension has several contributions. There are contributions from the propagation of momentum and interparticle forces of the DPD particles and they are given by

$$\sigma_{\alpha\beta} = \frac{1}{Vm}\sum_i \tilde{p}_{i\alpha}\tilde{p}_{i\beta} + \frac{1}{2V}\sum_{i,j} f_{ij}^{\alpha}(\mathbf{r}_i - \mathbf{r}_j)_{\beta}, \tag{2}$$

where i and j refer to two different DPD particles, α and β refer to Cartesian coordinate axes, f_{ij} is the force between particles i and j, and $\tilde{p}_i$ is the momentum of particle i relative to the macroscopic velocity field. V is the total volume of the system and m is the mass of the DPD particles. In addition there are contributions from the colloidal interactions. The stress contribution from the van der Waals forces is given by

$$\frac{1}{2V}\sum_{A,B} \mathbf{F}_{AB}^{\alpha}(\mathbf{r}_A - \mathbf{r}_B)_{\beta}, \tag{3}$$

where A and B refer to two different colloids and F_{AB} refer to the van der Waals forces between colloids A and B described above. Stress contributions from the lubrication forces are also included. They imply several modes. The most important one is the squeeze mode, which accounts for forces that develop as two spheres directly approach each other. This force is proportional to the velocity difference between the spheres and is inversely proportional to the nearest surface to surface distance. For the case of monosize spheres the lubrication force

$$F_{lub} = \tfrac{3}{2}\pi\eta a^2(\mathbf{v}_A - \mathbf{v}_B)/s_{AB}, \tag{4}$$

where η is the continuous fluid viscosity, a is the sphere radius, $\mathbf{v_A}$ is the velocity of colloid A, and s_{AB} is the nearest surface to surface distance between spheres A and B. Additional contributions to the squeeze mode as well are other modes all scale logarithmically and are largely dominated by the squeeze mode [20]. In our computations, all the modes of the lubrication force are taking into account up to the first order, including terms that scale as $1/s_{AB}$, $\ln s_{AB}$, and $s_{AB}\ln s_{AB}$.

There are additional corrections to the stress tensor due to the constraint forces on the DPD particles that make up the colloid. The constraint forces are determined by accounting for the rigid body motion in the individual particle displacements and change in velocity at each time step of the velocity-Verlet algorithm. Details of this approach are described in [23].

We study three volume concentrations, ϕ=20%, 40%, and 50%, where the number of colloidal particles ranges from 3760 to 9616. As we are interested in the onset of flow we study flow in a simple shear geometry with shear strain γ smaller than 1. In each simulation, we control the shear rate $\dot{\gamma}$ and measure the macroscopic stress σ.

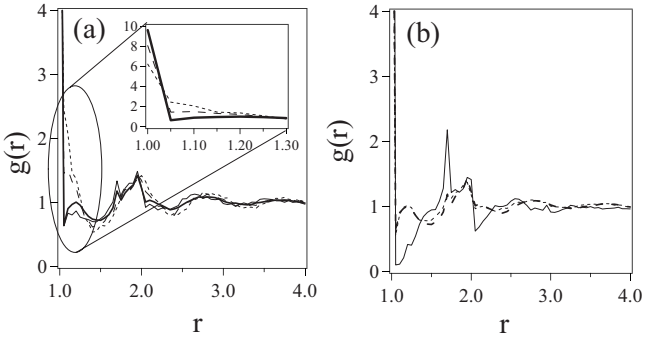

FIG. 4. (a) Evolution of the pair distribution function as a function of aging time for ϕ=50%, t_w=0.93 (short dashed line), t_w=9.3 (long dashed line), t_w=560 (continuous line), and t_w=1120 (thick continuous line). *Inset:* the pair distribution functions for the three studied aging times for particles close from contact. (b) Pair distribution function of the suspensions after tw=1120 for ϕ=20% (continuous line), ϕ=40% (short dashed line), and ϕ=50% (long dashed line).

III. PREPARATION OF THE SAMPLE

The colloidal particles are attractive, and in the absence of flow, the suspension evolves to form a colloidal gel. We follow a well-defined preparation protocol of the suspension. It is prepared by randomly placing the spheres, in a cubic cell, with small overlaps being possible. Then, a repulsive force is applied between spheres if they overlap. Once all the spheres no longer overlap, the system is allowed to equilibrate under the action of Brownian and hydrodynamic forces. As the system equilibrates, the pair distribution function is evaluated and found to become reasonable consistent with the Percus Yevick [24] approximation. When a stable radial distribution function is obtained, the van der Waals and lubrication forces are introduced by turning them on slowly enough so that the additional kinetic energy produced in the system, because two spheres are too close each other, is allowed to dissipate. We choose the end of the introduction of the van der Waals and the lubrication forces as the initial time of the system. Then, for a given time t_w (t_w=9.3, 93, or 1120), the suspension is allowed to evolve toward a flocculated colloidal gel. As the suspension ages during a time t_w, it is still out of equilibrium, and during this period, the pair distribution function evolves [Fig. 4(a)]: it becomes increasingly peaked at contact and develops secondary peaks. The increase in $g(r)$ at contact with time [Fig. 4(a), inset] is indicative of the increase in number of colloids in near contact [25]. For ϕ=20%, a marked peak at a distance between colloids' center equal to $\sqrt{3}r$ is obtained, showing that a local hexagonal structure develops [Fig. 4(b)].

IV. RESCALING OF THE FLOW CURVES

At several t_w values, we then begin to make the suspension flow. A shear deformation is imposed by translating the upper and lower boundaries of the cube according to the Lees-Edwards boundary condition [26]. The direction of the flow is denoted by $\mathbf{u_x}$ and its gradient $\mathbf{u_y}$ (Fig. 1). In order to compare our results with measured stress and shear rate val-

ues, we need to identify the characteristic stress $\tilde{\sigma}$ and time (or shear rate $\tilde{\dot{\gamma}}$) units of the flow. As the interparticle interaction is strong, the relevant energy scale in our system is the interaction potential between two particles rather than thermal energy, so that in the studied flow regime the interaction forces between two particles compete with hydrodynamic forces. Given that $F_{\max}$ is the maximal interaction force between two colloids, a is their radius, and η is the viscosity of the continuous medium, the natural stress and shear rate (and thus also time) units of our flow are given by

$$\tilde{\sigma} = \phi^2 \frac{F_{\max}}{a^2}, \tag{5}$$

$$\tilde{\dot{\gamma}} = \frac{F_{\max}}{6\pi\eta a^2}, \tag{6}$$

where $\tilde{\sigma}$ is the product of $F_{\max}$ with the number of particle bonds that cross the unit area, ϕ^2/a^2 [27] and $\tilde{\dot{\gamma}}$ is the shear rate, which equilibrates the intercolloidal stress, $F_{\max}/a^2$, with the hydrodynamic stress, $6\pi\eta\dot{\gamma}$. Our simulation results may thus be compared to real systems in which the energy of interactions between colloids is larger than thermal energy. Considering the 100 nm alumina particles, the maximal interaction force, given by the maximum of the slope of the interaction potential, is of the order of 4×10^{-13} N, so that the stress scale $\tilde{\sigma}$ is 40 Pa. The corresponding shear rate $\tilde{\dot{\gamma}}$ is 210 s^{-1}.

The response of the suspension to the application of shear is given in Fig. 5. At extremely low deformations, we do observe an elastic regime, in which the stress is proportional to strain and goes to zero at null shear values. Nevertheless, thermal activation plays a role in this elastic regime as the apparent elastic modulus measured decreases when the shear rate decreases. For this paper, we are not interested in this elastic regime but will describe in detail the onset of flow regime. The value of the stress at the onset of flow depends on the equilibrium time: the longer t_w, the higher the initial stress value. Then, the stress progressively increases up to a maximum value that does not depend on the equilibration time.

In addition, the stress growth curves of low concentration suspensions exhibit a remarkable feature: if the origin of strain is chosen to take a nonzero value, γ_0, then all the stress, as a function of strain, superimpose (Fig. 5, right column). γ_0 is an increasing function of the waiting time t_w. As a consequence, the application of flow plays the same qualitative role as the aging of the suspension. Such self-similarity is characteristic of the aging dynamics of out of equilibrium systems and has been observed in the case of concentrated soft colloidal particles [28].

In contrast to the low concentration suspensions, for the higher concentrations studied and when the waiting time is long enough, the evolution of the stress as a function of time exhibits a different shape. In this case, the stress growth curves may no longer be superimposed by shifting the strain. At long waiting times, the value of the stress (ignoring the elastic regime) at null strain now tends toward a nonzero finite value. The stress, needed to make the suspension flow, exceeds that which would be necessary according to the aging behavior. This departure from the scaling behavior occurs once the flow of the suspension has been started but before the establishment of a steady flow regime at larger shear values. The excess of stress, relative to the scaling behavior, needed to make the suspension flow thus differs from the idealized concept of yield stress, which is a nonzero value of the stress required to induce the flow, as $\dot{\gamma}\to 0$, and we call this excess stress a "supplementary stress." The higher the suspension concentration and the higher the shear rate, the greater the supplementary stress needed. As yield stress is generally associated with the breakage of bonds between attractive particles [4], we look for the microscopic origin of the supplementary stress that we measure macroscopically and consider the following:

(i) the evolution of the number of contacts between particles when shear is applied,

(ii) the orientation of contacts under shear, and

(iii) the angular distribution of interparticle stress between particles in contact.

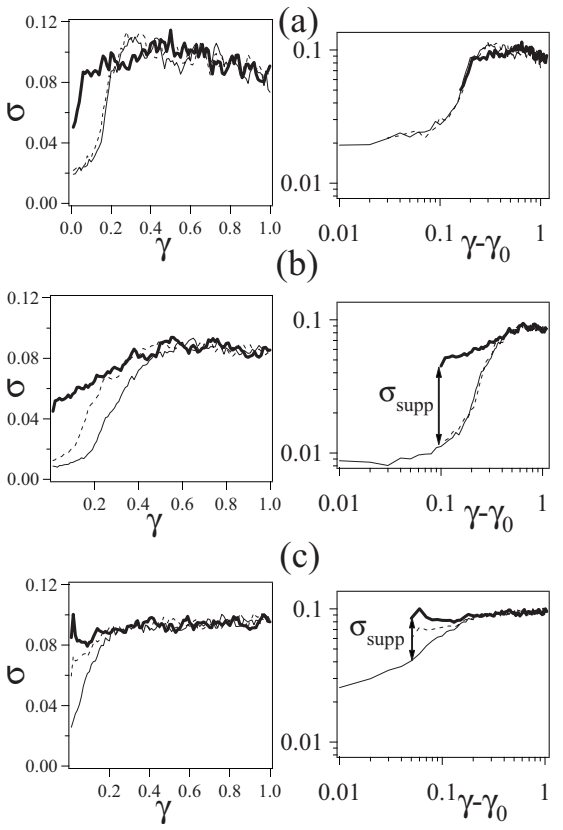

FIG. 5. (a)–(c) Dimensionless stress as a function of strain (left column) and shifted strain (right column) when a constant shear rate is applied ($\dot{\gamma}=3.5\times10^{-3}$). (a) $\phi=20\%$, (b) $\phi=40\%$, and (c) $\phi=50\%$. Before the application of shear, the suspension was allowed to equilibrate for times $t_w=9.3$ (continuous line), $t_w=93$ (dashed line), or $t_w=1120$ (bold continuous line). When the shear scale is translated by γ_0 (right column), all the curves superimpose at low concentration and exhibit a supplementary stress σ_{supp} at the two largest concentrations.

V. MICROSTRUCTURAL ORIGIN OF THE SUPPLEMENTARY STRESS

A. Evolution of the number of contacts

The microstructure of the suspension may be described with the help of the pair distribution function, $g(r)$. We have observed that it exhibits a first peak at contact, near $r=2a$, and a series of two correlation peaks. As the stress is localized in the thinnest gaps between particles [29], we focus our analysis on the particles in near contact and consider the pair distribution function $g(r)$ of the suspensions at different times as the suspension equilibrates and as the suspension is later strained. First note that $g(r)$ exhibits a well-defined maximum near $r=2a$, where the particles are at contact. From the value of this maximum, one can compute the average number of contacts Z of the particles [30,31],

$$Z = \frac{N}{V}\int_{2a}^{2a+\delta a} 4\pi r^2 g(r) dr, \tag{7}$$

with a being the radius of the particles, δa being the width of the first peak of the pair distribution function, N being their number, and V being the volume of the shearing cell. In the absence of flow, whatever the volume fraction, the number of contacts increases with time. Its initial value, at $t_w=0$, is very sensitive to the peculiar configuration of the considered suspension. Then, at long waiting times, it tends toward a plateau value close to 7. The higher the concentration and the longer the equilibrium waiting time, the faster the plateau value of Z is reached. When we apply a low shear rate, the number of contacts generally increases with time. On the contrary, at high shear rates, the total number of contacts decreases as time elapses before reaching an equilibrium. Whatever the applied shear rate value, we found that the evolution of the number of contacts as a function of the shear follows a simple exponential behavior (Fig. 6): $Z(\gamma)=Z_\infty+(Z_0-Z_\infty)e^{-\gamma/\gamma_c}$, where Z_0 is the number of contacts before the application of shear, Z_∞ is the number of contacts once equilibrium is established, and γ_c is a characteristic strain of contact formation (at low shear rate) or contact disruption (at high shear rates). At low shear rate, γ_c is of the order of 100%, corresponding to the characteristic shear necessary to induce collision between two colloids. γ_c thus decreases when the volume fraction of the suspension increases [Fig. 6(d)]. In contrast, at higher shear rates, the number of contacts decreases and disruption of contacts dominates the dynamics. Here, γ_c no longer depends on the volume fraction of the suspension [Fig. 6(d)]. Whatever the volume fraction and the shear rate, the evolution of the number of contacts as a function of shear is always a simple exponential function and we do not observe a significant increase in the contact number that could be responsible for the nonscaling behavior of the flow curves when the suspension has aged long enough.

B. Orientation of contacts

The evolution of the number of contacts alone cannot explain the appearance of a supplementary stress. We next consider their orientation relative to the shear direction. We do not observe any orientation of the direction of contacts either in the plane normal to the shear direction or in the plane normal to the shear. In the shear/shear gradient plane, the contacts become anisotropic under flow (Fig. 7). A very different behavior is observed at low and at high volume fractions. Indeed, for $\phi=20\%$ and 40%, the ratio of the number of contacts in the compression quadrant over those in the extension quadrant, N^{comp}/N^{ext}, decreases when the shear increases. On the contrary, for the highest volume fraction, $\phi=50\%$, it increases. This observation agrees with experimen-

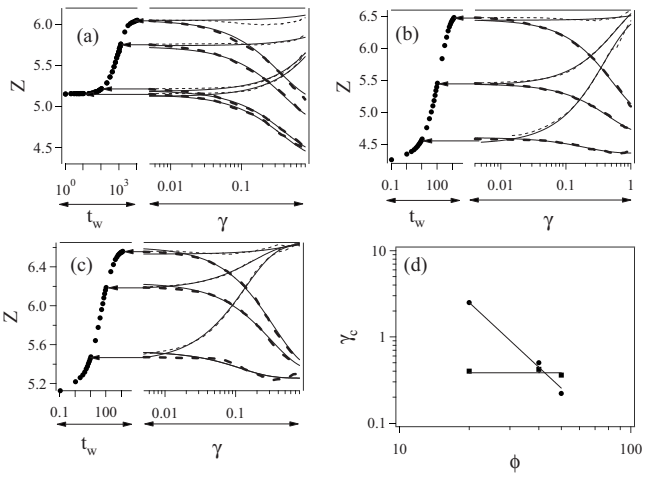

FIG. 6. Evolution of the number of contacts as a function of t_w before the application of shear rate (●) and under flow as a function of the shear γ for three volume fractions, (a) $\phi=20\%$, (b) $\phi=40\%$, and (c) $\phi=50\%$. Two shear rate values are represented: $\dot{\gamma}=3.5\times10^{-3}$ (thin dashed lines) and $\dot{\gamma}=3.5\times10^{-1}$ (thick dashed lines). Continuous lines are exponential fits of the data, $Z(\gamma)=Z_\infty+(Z_0-Z_\infty)e^{-\gamma/\gamma_c}$. (d) Critical shear values deduced from the monoexponential fits at $\dot{\gamma}=3.5\times10^{-3}$ (●) and $\dot{\gamma}=3.5\times10^{-1}$ (■) as a function of the volume fraction, ϕ.

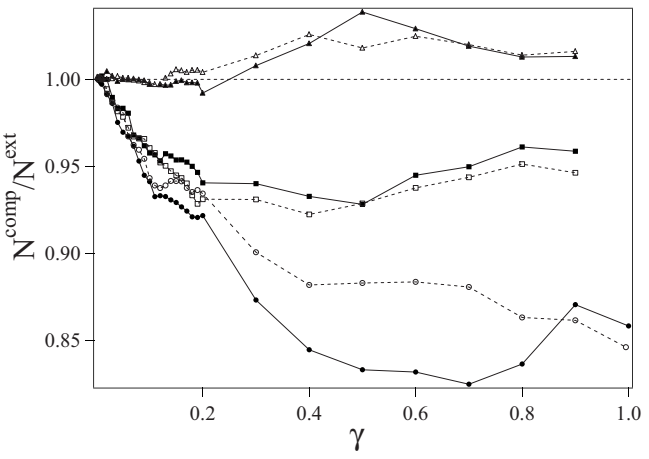

FIG. 7. Evolution of the ratio of contacts in the compression quadrant over the contacts in the extension quadrant, as a function of shear, for $\phi=20\%$ (circles), $\phi=40\%$ (squares), and $\phi=50\%$ (triangles). Solid lines and filled symbols (dashed lines and empty symbols) correspond to suspensions that have aged for $t_w=9.3$ ($t_w=1120$).

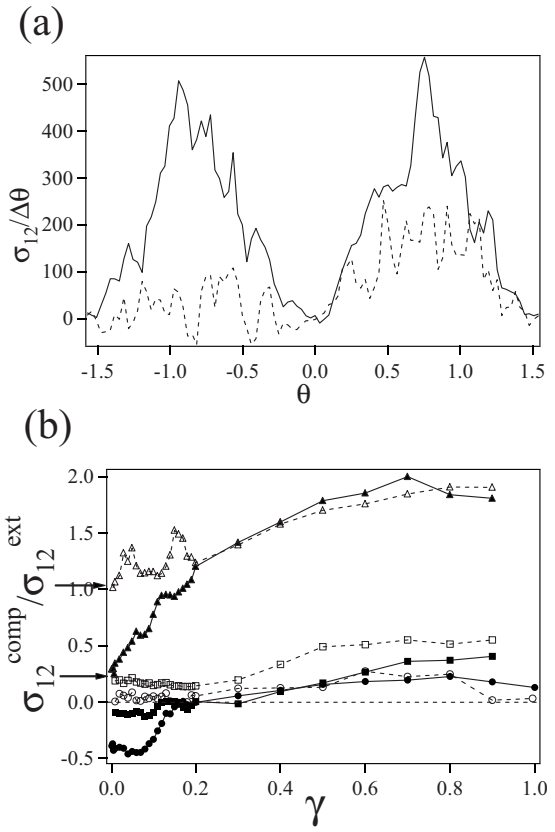

FIG. 8. (a) Angular distribution of the stress between contacts (stress σ_{12} localized along contacts that form an angle $[\theta, \theta+\Delta\theta]$ with the flow direction (see Fig. 1), with $\Delta\theta=\pi/180$, for a suspension whose volume fraction is $\phi=50\%$ and after a shear of 0.05. Dashed lines (continuous lines) correspond to suspensions that have aged for $t_w=9.3$ ($t_w=1120$). (b) Evolution of the ratio of stress stored along contacts in the compression quadrant over the stress stored along contacts in the extension quadrant, as a function of shear, for $\phi=20\%$ (circles), $\phi=40\%$ (squares), and $\phi=50\%$ (triangles). Continuous lines and filled symbols (dashed lines and empty symbols) correspond to suspensions that have aged for $t_w=9.3$ ($t_w=1120$). Arrows point at the nonzero limits of the stress ratio, at $\phi=40\%$ and $\phi=50\%$, and $t_w=1120$.

tal observation of the formation of aggregates in the compression quadrant, close to the direction of the flow [2].

More remarkably, the contact anisotropy curves for $t_w=9.3$ and $t_w=1120$ superimpose (Fig. 7), whereas the measured macroscopic stresses exhibit very different behavior, the longest aged suspension no longer obeying to the scaling behavior. Once again, this observation rules out the hypothesis that the contact anisotropy is responsible for the excess of stress.

C. Angular distribution of interparticle stress between particles in contact

We thus consider the anisotropy of the stress stored between contacts and define $\sigma_{12}^{comp}/\sigma_{12}^{ext}=\int_{-\pi/2}^{0}\sigma_{12}(\theta)d\theta/\int_{0}^{\pi/2}\sigma_{12}(\theta)d\theta$, the ratio of stress between contacts in the compression over the extension quadrant. The stress between contacts for the highest concentrated and longest aged suspension ($\phi=50\%$, $t_w=1120$) accumulates

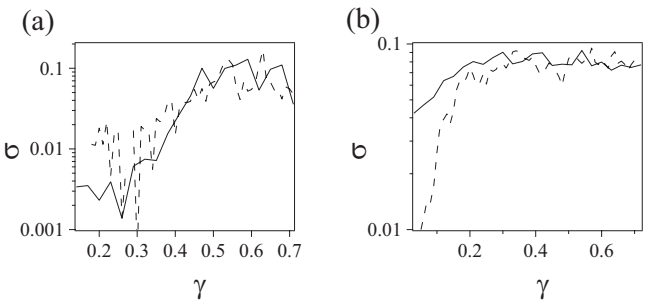

FIG. 9. Stress as a function of strain for two different volume fractions, (a) $\phi=20\%$ and (b) $\phi=50\%$. Continuous lines correspond to an interaction potential between colloids whose minimum values $U_{\min}$ are $25k_BT$ (continuous lines) and $125k_BT$ (dashed lines). The stress curves for $U_{\min}=125k_BT$ have been divided by 4.6 ($\phi=20\%$) and 3.2 ($\phi=50\%$) in order to match the stress curves for the less deep minimum of interaction potential ($U_{\min}=25k_BT$).

in the compression quadrant of the flow, whereas stress is only localized in contacts oriented in the extension quadrant for the less aged suspension [Fig. 8(a)]. More generally, for $\phi=40\%$ and $\phi=50\%$, the stress along contacts in the compression quadrant no longer tend toward 0 when the strain γ goes to 0 [Fig. 8(b)]. Thus, the macroscopic stress necessary to induce the flow is stored along contacts oriented in the compression quadrant. This result is important as it complements the general observation that the yield stress is due to the breaking of contacts in the extension direction [4]. As shown in Fig. 8(a), for concentrated flocculated suspensions, the creation of contacts and their setting under tension in the compression quadrant of the flow is quantitatively as important as their breaking in the extension direction [32].

A macroscopic consequence of the creation and disruption of contacts between colloids may also be found in the evolution of the stress with strain of the suspension when the depth of the van der Waals potential minimum is different. We have performed simulations for $\phi=20\%$ and $\phi=50\%$ for two different interaction potential depths, $25k_BT$ and $125k_BT$. Although one may expect that the maximum stress would increase by the same factor of the depth of the interaction potential between colloids, we observe that while it increases by a factor of 4.6 for $\phi=20\%$, there is only a factor of 3.7 increase for $\phi=50\%$ (Fig. 9). This indicates that some stress is not only due to the van der Waals interaction between the colloids but also due to the creation and disruption of contacts as the colloids rearrange themselves under shear. Such forces play a larger role when the suspension is more concentrated.

VI. CONCLUSION

In summary, the beginning of the application of shear strain to a colloidal suspension induces an anisotropy of the orientation of contacts between particles. This anisotropy is qualitatively different at low and high volume fractions. In the first case, an excess of contacts develop, whose relative orientation lies in the extension quadrant of the shear flow, and in the latter, there is an increase in particles whose relative orientation is in the compression quadrant. At low volume fractions, the stress necessary to induce flow is the

stress needed to break bonds, and microscopic stress is stored in the extension quadrant, which corresponds to the standard explanation of the origin of yield stress. Nevertheless, at high volume fraction, a new physical mechanism plays a role in the appearance of yield stress: the accumulation of stress in the compression quadrant of the flow.

ACKNOWLEDGMENTS

We would like to gratefully acknowledge support from the Virtual Cement and Concrete Testing Laboratory Consortium. The flow simulations were performed under Award No. SMD-05-A-0129, "Modeling the Rheological Properties of Suspensions: Applications to Cement Based Materials" for NASA's National Leadership Computing System Initiative on the "Columbia" supercomputer at the NASA Ames Research Center. This research used resources of the Argonne Leadership Computing Facility at Argonne National Laboratory, which is supported by the Office of Science of the U.S. Department of Energy under Contract No. DE-AC02-06CH11357.

[1] P. Varadan and M. J. Solomon, J. Rheol. **47**, 943 (2003).
[2] B. J. Maranzano and N. J. Wagner, J. Chem. Phys. **117**, 10291 (2002).
[3] P. Schall, D. A. Weitz, and F. Spaepen, Science **318**, 1895 (2007).
[4] R. G. Larson, *The Structure and Rheology of Complex Fluids* (Oxford University Press, New York, 1999).
[5] H. A. Barnes, J. Rheol. **33**, 329 (1989).
[6] J. Bender and N. J. Wagner, J. Rheol. **40**, 899 (1996).
[7] D. Lootens, H. Van Damme, and P. Hébraud, Phys. Rev. Lett. **90**, 178301 (2003).
[8] H. A. Barnes and K. Walters, Rheol. Acta **24**, 323 (1985).
[9] P. C. F. Møller, J. Mewis, and D. Bonn, Soft Matter **2**, 274 (2006).
[10] J. R. Stokes and J. H. Telford, J. Non-Newtonian Fluid Mech. **124**, 137 (2004).
[11] E. Somfai and L. M. Sander, Phys. Rev. E **56**, R5 (1997).
[12] T. Serra, J. Colomer, and X. Casamitjana, J. Colloid Interface Sci. **187**, 466 (1997).
[13] R. J. Flatt, N. Martys, and L. Bergstrom, MRS Bull. **29**, 314 (2004).
[14] N. S. Martys, J. Rheol. **49**, 401 (2005).
[15] P. Español and M. Revenga, Phys. Rev. E **67**, 026705 (2003).
[16] P. J. Hoogerbrugge and J. M. V. A. Koelman, Europhys. Lett. **19**, 155 (1992).
[17] R. D. Groot and P. B. Warren, J. Chem. Phys. **107**, 4423 (1997).
[18] P. Español and P. Warren, Europhys. Lett. **30**, 191 (1995).
[19] E. Boek, P. V. Coveney, H. N. Lekkerkerker, and P. Van der Schoot, Phys. Rev. E **55**, 3124 (1997).
[20] S. Kim and S. J. Karrila, *Microhydrodynamics* (Butterwort-Heinemann, Stoneham, MA, 1991).
[21] D. R. Foss and J. F. Brady, J. Fluid Mech. **407**, 167 (2000).
[22] J. N. Israelachvili, *Intermolecular and Surface Forces* (Academic, London, 1973.
[23] N. S. Martys, Phys. Rev. E **59**, 3733 (1999).
[24] T. M. Reed and K. E. Gubbins, *Applied Statistical Mechanics: Thermodynamics and Transport Properties of Fluids* (Butterwort-Heinemann, Stoneham, MA, 1991).
[25] R. J. M. d'Arjuzon, W. Frith, and J. R. Melrose, Phys. Rev. E **67**, 061404 (2003).
[26] M. P. Allen and D. J. Tildesley, *Computer Simulation of Liquids* (Clarendon, Oxford, 1987).
[27] W. B. Russel, D. A. Saville, and W. R. Schowalter, *Colloidal Dispersions* (Cambridge University Press, Cambridge, 1989).
[28] M. Cloitre, R. Borrega, and L. Leibler, Phys. Rev. Lett. **85**, 4819 (2000).
[29] L. E. Silbert, R. S. Farr, J. R. Melrose, and R. C. Ball, J. Chem. Phys. **111**, 4780 (1999).
[30] J.-P. Hansen and I. R. MacDonald, *Theory of Simple Liquids* (Academic Press, New York, 1976).
[31] T. Aste, M. Saadatfar, and T. J. Senden, Phys. Rev. E **71**, 061302 (2005).
[32] D. Lootens, H. van Damme, Y. Hémar, and P. Hébraud, Phys. Rev. Lett. **95**, 268302 (2005).